

## Formation and stability of tripolar vortices in stratified geostrophic flows (\*)(\*\*)

S. M. CORRÉARD and X. J. CARTON

*French Navy Oceanographic Center (SHOM/CMO) - 29275 Brest, France*

(ricevuto il 18 Novembre 1998; approvato il 6 Maggio 1999)

**Summary.** — The formation, stationarity and stability of tripolar vortices is investigated in a two-layer quasi-geostrophic model. On the  $f$ -plane, these tripoles form from the barotropic and baroclinic instabilities of circular isolated vortices. Various horizontal and vertical potential vorticity distributions, both piecewise-constant and continuous, are considered here for these circular vortices. First, their linear stability is computed for normal-mode perturbations. Then, their nonlinear evolution with an elliptical initial perturbation is studied by means of a pseudo-spectral and of a contour surgery code. Two types of baroclinic tripoles are found to result from these instabilities: surface-intensified structures for dominant barotropic instability, arch-shaped tripoles for more baroclinic vortices. The stationarity of these tripoles and their stability to initial disturbances or to the action of beta-effect is finally investigated.

PACS 92.10.Ei – Coriolis effects.

PACS 47.20 – Hydrodynamics stability.

PACS 47.32.Cc – Vortex dynamics.

PACS 47.55.Hd – Stratified flows.

PACS 01.30.Cc – Conference proceedings.

### 1. – Introduction

Much effort has been devoted lately to understand the stability of geostrophic vortices [1-3]. In particular, barotropically unstable vortices, once elliptically deformed, can stabilize nonlinearly as long-lived tripoles [4-7]. In two-layer quasi-geostrophic flows, purely baroclinic, shielded Gaussian vortices can form counter-rotating, pulsating ellipses when unstable on an elliptic mode; these ellipses do not reach a stationary state [8]. The purpose of the present study is to investigate if stationary and

---

(\*) Paper presented at the International Workshop on “Vortex Dynamics in Geophysical Flows”, Castro Marina (LE), Italy, 22-26 June 1998.

(\*\*) The authors of this paper have agreed to not receive the proofs for correction.

long-lived baroclinic tripoles, both with continuous and piecewise-constant potential vorticity distributions can exist in a two-layer quasi-geostrophic model.

After recalling the quasi-geostrophic equations and nonlinear numerical models that we use in this study (sect. 2), we describe the formation and evolution of baroclinic tripoles with continuous potential vorticity distributions (sect. 3). Then we consider piecewise-constant vortices, for which the growth rates of normal-mode perturbations can be computed analytically. The nonlinear evolutions of such vortices, elliptically perturbed, are then computed. The tripoles which result from these evolutions are compared with exact stationary states (sect. 4). Finally, the stability of baroclinic tripoles to initial perturbations or to the planetary vorticity gradient is evaluated (sect. 5).

## 2. – The quasi-geostrophic equations and numerical models

The quasi-geostrophic dynamics is governed by an evolution equation for the total (potential and planetary) vorticity. In a two-layer model, this equation is

$$(1) \quad \frac{d(q_j + f)}{dt} = \partial_t q_j + J(\psi_j, q_j) + \beta \partial_x \psi_j = \nu \nabla^6 \psi_j,$$

where the right-hand side is the hyperviscosity, used in the spectral model (see hereafter). The layerwise streamfunction is  $\psi_j$ ; the two-dimensional advecting velocity is  $\vec{u}_j = k \wedge \nabla \psi_j$  and the potential vorticity is

$$(2) \quad q_j = \nabla^2 \psi_j + \frac{f_0^2}{g' H_j} (\psi_k - \psi_j), \quad k = 3 - j.$$

The (upper, lower) layer index is  $j = 1, 2$ . The reduced gravity is  $g' = g(\varrho_2 - \varrho_1/\varrho_0)$  where  $\varrho_j$  is the density in layer  $j$  and  $\varrho_0$  its vertical average; the Coriolis parameter is  $f = f_0 + \beta y$ , and  $\beta = 0$  here, except in sect. 5; finally, we note  $h_j = H_j/H$  the fractional thickness of layer  $j$ . The internal radius of deformation is given by  $R_d^2 = g' H(h_1 h_2)/f_0^2$ . Hereafter, we write  $\gamma^2 = 1/R_d^2$ .

Two numerical models are used to investigate the nonlinear evolution of unstable vortices: 1) a pseudo-spectral code for continuous vortices on a biperiodic square grid ( $L = 4\pi$ ), with  $128^2$  nodes and  $\nu = 10^{-7}$  to remove enstrophy accumulation at small scales; 2) an inviscid contour surgery code [8] on an infinite plane for piecewise-constant vortices. Equal layer thicknesses are used here ( $h_1 = h_2 = 0.5$ ). Note that in this case, the triadic interaction coefficient of the baroclinic mode vanishes. Therefore, we have checked that the results presented here are qualitatively similar for unequal layer thicknesses ( $h_1 = 0.2, h_2 = 0.8$ ); in particular, tripole formation also occurs, though baroclinic instability is more efficient then.

## 3. – Baroclinic tripoles with continuous potential vorticity

To create baroclinic tripoles with continuous potential vorticity, we study the instability of the following vortex family:

$$(3) \quad \nabla^2 \bar{\psi}_j(r) = \bar{A}_j \left( 1 - \frac{\alpha}{2} r^\alpha \right) \exp[-r^\alpha]$$

with  $\bar{A}_1 = 1, \bar{A}_2 = \kappa$ . This family of isolated vortices, often used [4, 5, 7, 9], includes Gaussian ( $\alpha = 2$ ) and cubic exponential ( $\alpha = 3$ ) vortices, both of interest for oceanic and laboratory applications. Note that  $\alpha$  parameterizes the horizontal vorticity shear, and  $\kappa$  the vertical one. The vortex radius is here set to unity, the scaling factor in the exponential; note that this is not the radius of maximum velocity (which is  $R_v = (1/\alpha)^{1/\alpha}$ ).

To compute the growth rate of elliptical perturbations on these vortices, the potential vorticity equation (1) is linearized around the circular flow to form the Rayleigh equation,

$$(4) \quad (\bar{U}_j - c) q'_j - \frac{d\bar{q}_j}{dr} \psi'_j = 0.$$

The perturbation is a normal mode  $\psi'_j(r, \theta) = A_j \text{Re}[f_j(r) \exp[i l(\theta - ct)]]$  with  $l = 2$ . The Rayleigh equation is discretized in  $r$  to form a generalized eigenvalue problem solved by a matrix method. This provides the growth rates  $\sigma = l\tilde{\mathcal{N}}(c)$ .

The results are shown in fig. 1 for  $\alpha = 3$  (calculations have been performed also for  $\alpha = 2$ , but the exponential cubic profile is more sensitive to barotropic instability and is retained here). First, we note that for  $\gamma^2 \sim 0$ , layers decouple and  $\sigma$  does not vary with  $\kappa$ . Then, when stratification increases, the growth rates decrease, all the more so as the vortex is vertically sheared. This is characteristic of barotropic instability. For deformation radii on the order of half the vortex radius ( $\gamma^2 = 4$ ), barotropic instability dominates in the interval  $\kappa \in [0.4, 1.0]$ . Still, for  $\gamma^2 \in [3; 4]$  and  $\kappa \in [-1.0, 0.0]$ , a region of baroclinic instability is found with growth rates increasing with  $\gamma^2$ .

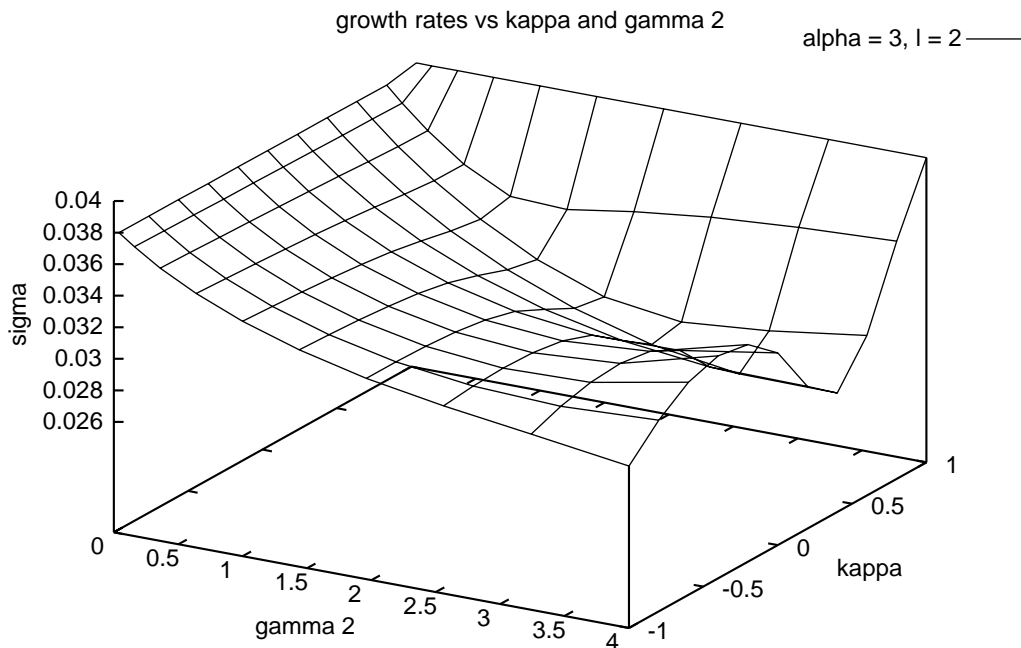


Fig. 1. – Growth rate of elliptical normal-mode perturbations on an isolated cubic exponential vortex with respect to the inverse squared deformation radius  $\gamma^2$  and to the vortex baroclinicity  $\kappa$ .

TABLE I. – *Nonlinear evolutions of the elliptically perturbed cubic exponential vortex, in the spectral code. The symbols are: NSTP: non-stationary tripole, STP: stationary tripole, TP+E: upper-layer tripole and perpendicular ellipse in the lower layer, (a): final asymmetric breaking of the whole structure, DPBK: dipolar breaking of the original vortex.*

$\gamma^2 \backslash \kappa$	-1.0	-0.75	-0.5	-0.25	0.0	0.25	0.5	0.75	1.0
0.25	NSTP	NSTP	NSTP	NSTP	STP	NSTP	NSTP	NSTP	STP
1.0	NSTP	NSTP	NSTP	NSTP	STP	NSTP	NSTP	NSTP	STP
2.25	NSTP	NSTP	NSTP	TP+E	TP+E	STP	STP	STP(a)	STP
4.0	DPBK	DPBK	DPBK	DPBK	TP+E	STP	STP	STP(a)	STP

Numerical experiments are then performed with the spectral code to determine the nonlinear evolutions of the elliptically perturbed vortex with  $\alpha = 3$  for  $\gamma^2 \in [0.25, 4.0]$ ,  $\kappa \in [-1.0, 1.0]$ . The results are summarized in table I. Essentially, four cases are found:

1) the vortex forms a tripole in the upper layer; in the lower layer, the vortex (a tripole or an ellipse) does not rotate with the same rate as the upper-layer tripole; the whole structure is not stationary (NSTP); this occurs mostly for baroclinic mean flows;

2) a tripole is formed in the upper layer. In the lower layer, the vortex forms an ellipse which elongates towards the upper-layer satellites (TP + E); this occurs for weak lower-layer flows and strong layer coupling;

3) the horizontal or vertical shear are too intense and break the vortex into dipoles (DPBK). This occurs for strong layer coupling and dominantly baroclinic vortices;

4) a tripole is formed in the upper layer; in the lower layer, the vortex (a tripole or an ellipse) rotates with the same rate as the upper-layer tripole; the whole structure is stationary (STP); this occurs for ( $\kappa = 0$ ,  $\gamma^2 \leq 1$ ), for ( $\kappa = 1$ ,  $\forall \gamma^2$ ) and for ( $0 < \kappa < 1$ ,  $\gamma^2 > 1$ ). Note that for  $\gamma^2 = 4.0$  two types of stationary tripoles are found:

– a surface-intensified one (for  $\kappa = 0.5$ , for instance): it consists in tripoles in both layers, with a stronger intensity in the upper layer;

– an “arch-shaped” one (for  $\kappa = 0$ ): a tripole is formed in the upper layer while the lower-layer (negative) vortex breaks into two lobes which align with the upper-layer satellites. Finally, we remark that asymmetric breaking of two-layer geostrophic tripoles occurs after a long model time, if they are nearly barotropic.

Figure 2a shows time series of potential vorticity maps for the vortex with  $\alpha = 3$  (simulations with the spectral code). The initial perturbation is elliptical and weak (0.5% amplitude); the physical parameters are  $\gamma^2 = 4.0$ ,  $\kappa = 0.5$ . An invariant tripole is formed in the upper layer first, while the lower-layer vortex is still adjusting. At time  $t = 9.6\tau$  (where  $\tau = 4\pi/\bar{A}_1$  is a turnover time of the initial vortex), filamentation is still intense in the lower layer: some of the core potential vorticity is entrained into the satellites, decreases their circulation and the shear they exert on the core; finally, the lower core axisymmetrizes and rolls up at  $t = 12.7\tau$ . This process is quite similar to that observed in two-dimensional tripole formation [7], though here the lower- and upper-layer dynamics are strongly coupled.

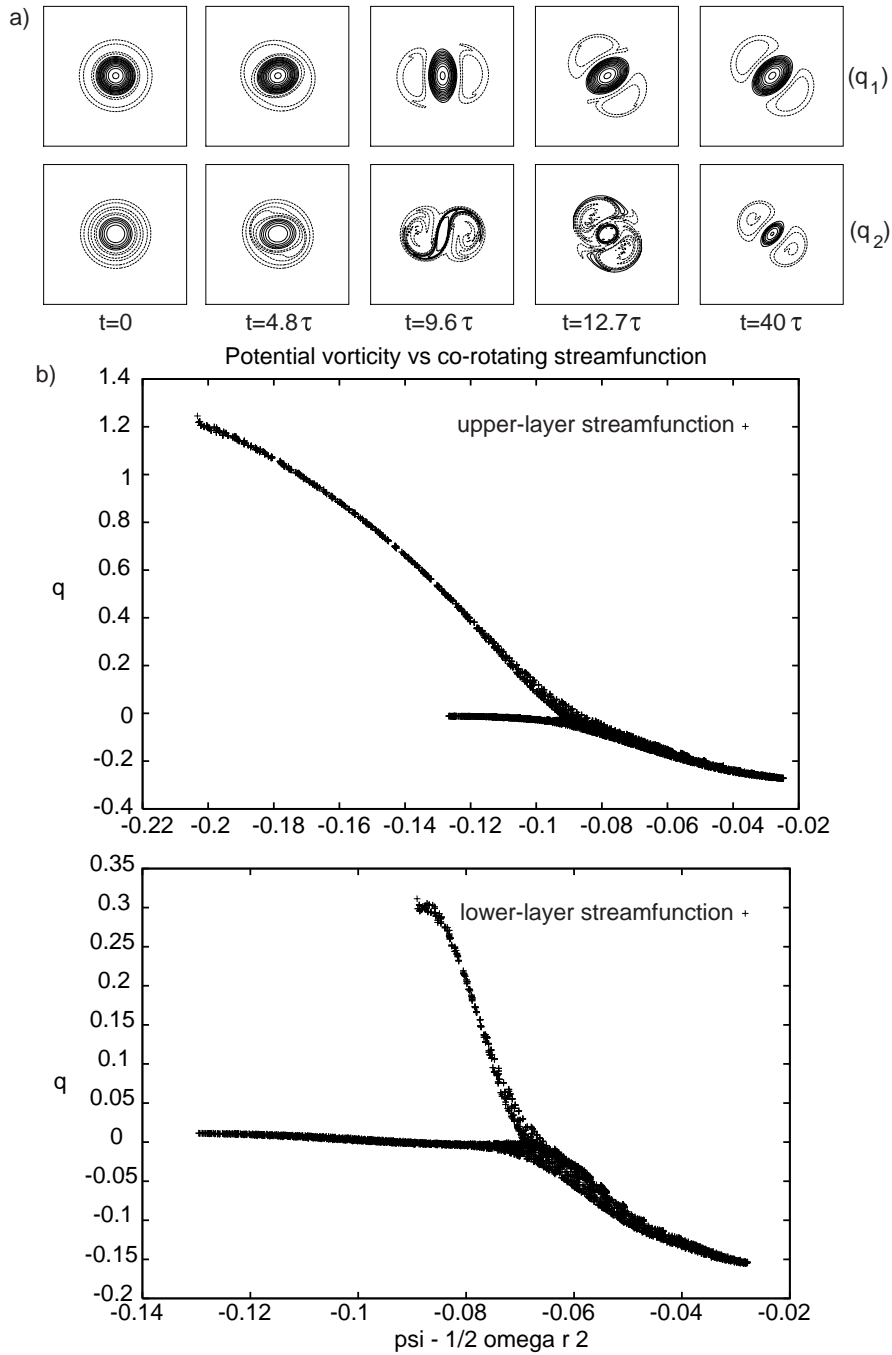


Fig. 2. – a) Time-series of potential vorticity maps in the spectral code, showing the formation of a stationary tripole from a cubic exponential vortex ( $\gamma^2 = 4.0$ ,  $\kappa = 0.5$ ). The top and bottom rows represent the upper and lower model layers. Shown are  $t = 0, 4.8\tau, 9.6\tau, 12.7\tau, 40\tau$ . b) Scatter-plots of potential vorticity *vs.* co-rotating streamfunction in both layers for the tripole of a).

Scatter plots of potential vorticity *vs.* corotating streamfunction in both layers is shown in fig. 2b. They have been obtained by averaging the vortex in the rotating frame of reference from  $t = 28.6\tau$  until  $t = 40\tau$ , with a rotation rate  $\Omega = 0.055$ . The weak scatter of points shows that the whole structure is indeed stationary.

#### 4. – Piecewise-constant baroclinic tripoles

4.1. *Formation.* – For a cubic exponential vortex, varying  $\gamma^2$  modifies the potential vorticity distribution in both layers, and changes the stability properties of the vortex. To remedy this, we consider here a vortex composed of three circular regions of constant (non-zero) potential vorticity, which do not vary with  $\gamma$ . In the upper layer, the vortex is composed of a central disk (radius  $R_1$  and potential vorticity  $q_1$ ), coaxial with a separate annulus (potential vorticity  $q_3$ , inner radius  $R_2$  and outer radius  $R_3$ ). In the lower layer, a disk of potential vorticity  $q_2 = \kappa q_1$ , has a radius  $R_1$  and is co-axial with the upper disk. Since the whole structure is isolated, radii and vorticities are related by  $h_1[q_1 R_1^2 + q_3(R_3^2 - R_2^2)] + h_2 q_2 R_1^2 = 0$ . Here we set  $q_1 = 1$  and  $R_1 = 1$  which give us space and time scales. We also set  $R_2 = 1.6$ ,  $R_3 = 2.6$  in agreement with observations of oceanic vortices in the Bay of Biscay, the swoddies [10].

First, the linear growth rates of normal-mode perturbations on these piecewise-constant vortices is calculated analytically, as in [2, 3, 7]. The results are shown in fig. 3, for  $\kappa \in [-1; 1]$ ,  $l \in [1, 6]$ . We observe that, for  $\kappa < 0$ , growth rates increase with  $\gamma$ , a characteristic of baroclinic instability. We also note that modes  $l = 2, 1, 3, 4 \dots$  are successively unstable when  $\gamma$  increases; in general, mode  $l = 1$  is not very unstable. For  $\kappa > 0$ , growth rates decrease with increasing  $\gamma$ , a characteristic of barotropic instability; indeed, the vorticity shear is horizontal then. In this case, only mode  $l = 2$  is unstable.

The nonlinear evolution of these piecewise-constant vortices is now investigated with a contour surgery algorithm. These vortices are initially perturbed by a small elliptical contour deviation (0.1%). Two values of  $\gamma$  are used ( $\gamma = 1.11; 1.66$ ); they correspond, respectively, to  $R_d = 22.5$  km (in the deep ocean in the Bay of Biscay) and to  $R_d = 15$  km (in the coastal ocean) for a swoddy radius  $R_1 = 25$  km. The nonlinear evolutions are summarized in table II.

For  $\gamma = 1.11$ , barotropic instability is dominant for  $\kappa > 0$ , while the vortices are both linearly and nonlinearly stable for  $\kappa \leq 0$ . For strong instability ( $\kappa \in [0.6; 1.0]$ ), the instability does not saturate at finite amplitude and the elliptical perturbation grows until it breaks the vortex into two horizontal dipoles. For a more moderate instability ( $\kappa \in [0.2; 0.6]$ ), nonlinear interactions stabilize the elliptical perturbation and a surface-intensified tripole is formed. It is composed of a surface tripole and of a lower-layer ellipse aligned with the upper core.

For  $\gamma = 1.66$ , baroclinic instability is stronger. In the absence of the upper-layer annulus ( $\kappa = -1$ ), the vortex stabilizes in each layer as an ellipse. These ellipses rotate in opposite directions, and their aspect ratios pulsate periodically, in the shear imposed by the other layer vortex. For  $\kappa = -0.75, -0.5$ , vertical dipolar breaking occurs: the upper-layer annulus breaks into two lobes with which the lower-layer vortex tends to align; this latter thus breaks into two pieces. The shear exerted by the satellites on the upper core is then sufficient to break it into two fragments. Note that this is a nonlinear process due to the interaction of potential vorticity poles, and not simply linear baroclinic instability. Indeed, for  $\kappa = -1$ , where the vertical shear is more intense, no

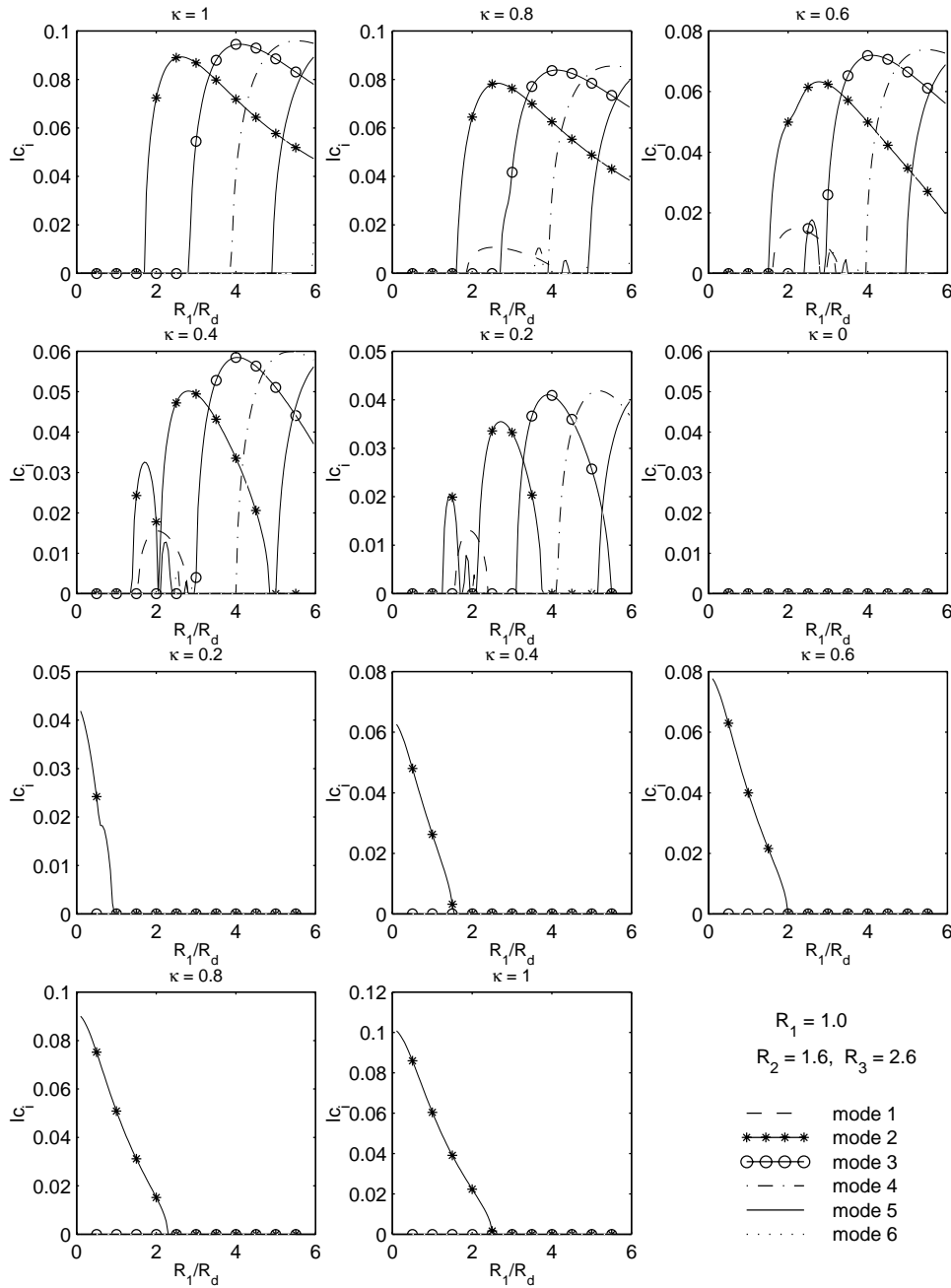


Fig. 3. – Linear stability diagrams for the isolated piecewise-constant vortex with  $q_1 = 1$ ,  $R_1 = 1$ ,  $R_2 = 1.6$ ,  $R_3 = 2.6$ . The growth rates of normal-mode perturbations are plotted vs.  $R_1/R_d$  for various values of  $\kappa$ .

TABLE II. – *Nonlinear evolutions of the elliptically perturbed piecewise-constant vortex, in the contour surgery code. The symbols are: STV: stable initial vortex, SITP: surface-intensified tripole, ASTP: arch-shaped tripole, HDP: horizontal dipolar breaking, VDP: vertical dipolar breaking, CRE: counter-rotating ellipses in the two layers.*

$\gamma^2 \backslash \kappa$	-1.0	-0.75	-0.5	-0.25	0.0	0.25	0.5	0.75	1.0
1.11	STV	STV	STV	STV	STV	SITP	SITP	HDP	HDP
1.66	CRE	VDP	VDP	ASTP	STV	STV	SITP	SITP	SITP

breaking is observed. For  $\kappa = -0.25$ , the vertical shear is less intense and the whole structure stabilizes as an arch-shaped tripole. Finally, for  $\kappa \in [0.5; 1.0]$ , surface-intensified tripoles are formed since the barotropic instability is less intense than for  $\gamma = 1.11$ .

Figure 4 presents the time series of potential vorticity maps for the formation of such a surface-intensified tripole with  $\gamma = 1.66$ ,  $\kappa = 0.5$  in the contour-surgery code. At early times, the upper- and lower-layer cores become elliptical and are vertically aligned; the upper-layer annulus breaks into two satellites. Then the upper-layer core is more sheared by the satellites than the lower-layer core; it filaments at its tips (where saddle points of the co-rotating streamfunction are located; see also [7]). Finally, at time  $t = 22.5\tau$ , filamentation has ceased and the tripole is formed, though weak disturbances are still observed on the contours, since the very weak dissipation cannot damp them rapidly.

4.2. *Stationary state.* – To determine if these piecewise-constant tripoles are stationary, we use an iterative algorithm designed by Wu *et al.*, in 1984 [11], and adapted to the present geometry. This algorithm calculates the steady states of two-layer surface-intensified tripoles from an initial guess of three circular vortices in the upper layer (one core and two satellites), and of one circular core vortex in the lower layer. These vortices are constrained to remain horizontally aligned in the upper layer, and symmetric with respect to both  $x$  and  $y$  axes in both layers. The two vortex cores must also remain vertically aligned. For each value of the distance between vortices, the vortex contours are iteratively adjusted until the velocity in the rotating frame of reference is tangential to them at every point. This relaxation is

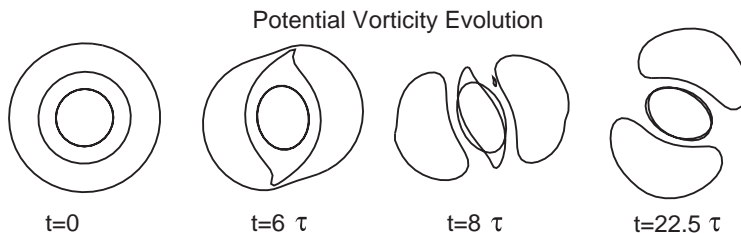


Fig. 4. – Time-series of potential vorticity maps in the contour surgery code showing the formation of a tripole from an unstable piecewise-constant with  $q_1 = 1$ ,  $R_1 = 1$ ,  $R_2 = 1.6$ ,  $R_3 = 2.6$  for  $\gamma = 1.66$ ,  $\kappa = 0.5$ . The upper- and lower-layer vorticity contours are superimposed here. Shown are  $t = 0, 6\tau, 8\tau, 22.5\tau$ .

based on a Newton-Raphson procedure. For a tripole, the final contours of the core are elliptical, and those of the satellites are “bean-shaped”.

The steady state thus obtained is similar to the end-state of the contour surgery simulation (not shown here). In particular, the differences in vortex areas are smaller than 5% for the upper-layer core and satellites, while the lower-layer core shows a 15% area difference between the two solutions. In fact, the satellites of the exact steady state are less deformed than those of the end-state of the contour surgery simulation. This difference can be attributed either to the limited dissipation in the contour surgery code which leaves contour disturbances to survive for long periods of time, or to the precision of the steady-state algorithm, which is of second order only. Fourth-order algorithms have obviously been shown to reproduce strongly curved contours more accurately, but they are computationally much more expensive (Wu *et al.*, [11]). Therefore, the tripole formed by the instability of the piecewise-constant vortex is quite close to the exact stationary solution.

## 5. – Stability of baroclinic tripoles

Finally, we investigate the robustness of baroclinic tripoles to initial disturbances and to the  $\beta$ -effect. First, the piecewise-constant tripole obtained in the previous section is introduced into the spectral code; the potential vorticity fronts are slightly smoothed to avoid numerical (Gibbs) instability. The stability of the tripole is first tested by adding a stochastic perturbation to the whole vorticity field (this perturbation is a white noise in relative vorticity). For maximum perturbation amplitudes of 0.02 to 0.2, the tripole is stable. For perturbation amplitudes of 0.3 to 0.6, the tripolar vortex emerges from the dissipating vorticity noise, but this tripole is not stationary and it becomes all the more asymmetric as the noise amplitude is large. The evolution of potential vorticity is shown in fig. 5a, for a 0.2 perturbation amplitude. The tripole, indistinguishable at first, rapidly readjusts under its stationary form.

Finally, the piecewise-constant tripole is used as an initial condition for the spectral code with  $\beta$ -effect (not shown here). On the beta-plane, all nonlinear evolutions show a

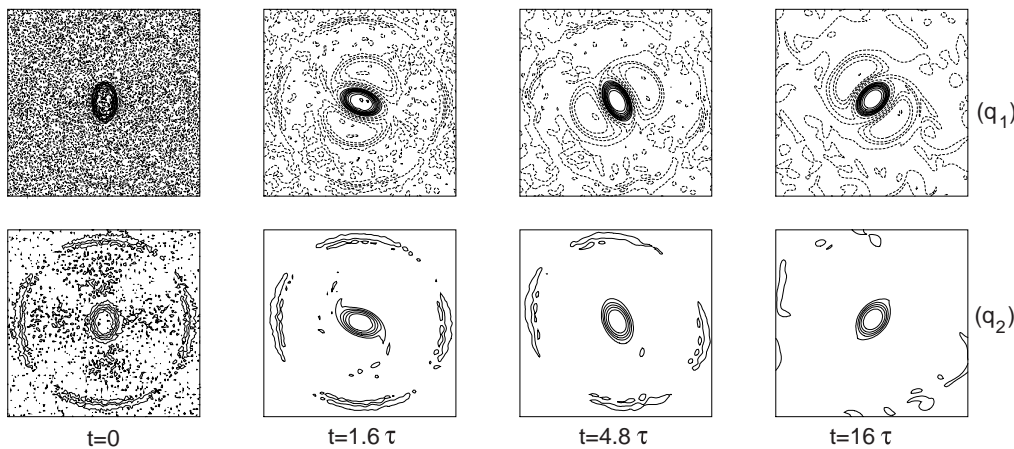


Fig. 5. – Time-series of potential vorticity maps in the spectral code, showing the evolution of the final tripole of fig. 3, perturbed with a 20% noise amplitude. Shown are  $t = 0, 1.6\tau, 4.8\tau, 16\tau$ .

TABLE III. – *Lifetime of the piecewise-constant baroclinic tripole shown in fig. 4, when evolving on the  $\beta$ -plane.*

$\beta$	0.005	0.01	0.02	0.03	0.04	0.05
$T_{\text{life}}$	$28.8\tau$	$20.8\tau$	$14.4\tau$	$11.2\tau$	$9.6\tau$	$8\tau$

northwestward drift of the tripole, accompanied by stretching-out and wrapping of the satellites around the core. After losing its satellites, the tripole reduces to its elliptical core vortex. Table III gives the time necessary to complete this process, for various values of  $\beta$ ; note that the time-scale  $\tau$  is the turn-over time of the initial circular vortex. Even for weak values of  $\beta$ , the decay of baroclinic tripoles is a fairly rapid process. Baroclinic tripoles are therefore unstable structures on the  $\beta$ -plane.

## 6. – Discussion and conclusions

Numerical experiments with a spectral and a contour surgery code have shown that baroclinic geostrophic vortices, linearly unstable on mode  $l=2$ , can stabilize nonlinearly as steadily rotating, symmetric tripoles on the  $f$ -plane. For both continuous and piecewise-constant vorticity distributions, two types of tripoles have been evidenced: surface-intensified and arch-shaped structures. The former are generated from more barotropic vortices than the latter. These tripoles are long-lived solutions of the two-layer quasi-geostrophic equations in the absence of  $\beta$ -effect. This latter induces an asymmetric breaking of baroclinic tripoles. On the  $f$ -plane too, piecewise-constant tripoles, which are robust in hyperviscous simulations (in the pseudo-spectral code), exhibit much more asymmetric instability in inviscid evolutions (*e.g.*, in a Contour-Advective Semi-Lagrangian code [12]). This is not explained as of now, especially since the linear instability diagram (fig. 3) does not evidence strong mode 1 instabilities. In fact, asymmetric instability has already been mentioned as a possible evolution of two-dimensional tripoles at late times [6, 7]. Further work should investigate this point in detail.

Other paths for future research on baroclinic tripoles include the extension of this study to intermediate-depths vortices in a multi-layer quasi-geostrophic model, for application to meddies (Mediterranean water eddies in the Atlantic ocean). Ageostrophic effects on the formation of tripoles should also be studied, for more realism in oceanic applications.

\* \* \*

The first author was supported by a research grant from SHOM/CMO. Special thanks are due to Prof. D. G. DRITSCHER (University of Warwick, UK) for sharing his CASL code. J. DA CRUZ and B. FORGEAU took an active part in the early research on this subject. Discussions with Prof. G. R. FLIERL (MIT/CMPO, USA) and Dr. Y. MOREL (SHOM/CMO, France) proved timely and valuable.

## REFERENCES

- [1] GENT P. R. and McWILLIAMS J. C., *Geophys. Astrophys. Fluid Dyn.*, **35** (1986) 209.
- [2] FLIERL G. R., *J. Fluid Mech.*, **197** (1988) 349.
- [3] HELFRICH K. R. and SEND U., *J. Fluid Mech.*, **197** (1988) 331.
- [4] CARTON X. J., FLIERL G. R. and POLVANI L. M., *Europhys. Lett.*, **9** (1989) 339.
- [5] ORLANDI P. and VAN HELJST G. J. F., *Fluid Dyn. Res.*, **9** (1992) 179-206.
- [6] VAN HELJST G. J. F., KLOOSTERZIEL R. C. and WILLIAMS C. W. M., *J. Fluid Mech.*, **225** (1991) 301-331.
- [7] CARTON X. J. and LEGRAS B. *J. Fluid Mech.*, **267** (1994) 53.
- [8] DRITSCHEL D. G. and R. SARAVANAN, *Q. J. R. Met. Soc.*, **120**, (1994) 1267.
- [9] CARTON X. J. and Mc WILLIAMS J. C., *Dyn. Atmos. Oceans*, **24** (1996) 207.
- [10] PINGREE R. and B. LECANN, *Deep-Sea Res.*, **39** (1992) 1147.
- [11] WU H. M., OVERMAN E. A. II and ZABUSKY N. J., *J. Comp. Phys.*, **53** (1984) 42.
- [12] DRITSCHEL D. G. and AMBAUM M. H. P., *Q. J. R. Meteorol. Soc.*, **123** (1997) 1097.